Kinetics of the isotope exchange reaction of 1 8O with NO and O2 at 298 K

S. M. Anderson, F. S. Klein, and F. Kaufman

Citation: The Journal of Chemical Physics **83**, 1648 (1985); doi: 10.1063/1.449402
View online: http://dx.doi.org/10.1063/1.449402
View Table of Contents: http://scitation.aip.org/content/aip/journal/jcp/83/4?ver=pdfcov
Published by the AIP Publishing

Kinetics of the isotope exchange reaction of ^{18}O with NO and O_2 at 298 K

S. M. Anderson, F. S. Klein,[a] and F. Kaufman
Department of Chemistry, University of Pittsburgh, Pittsburgh, Pennsylvania 15260

(Received 1 April 1985; accepted 2 May 1985)

The rates of ^{18}O isotope exchange reactions were measured at 298 K using a discharge-flow, modulated molecular beam mass spectrometer apparatus whose detection limit for NO and O was in the 10^9–10^{10} cm^{-3} range. The NO exchange is very fast, $k_{1,x} = (3.7 \pm 0.5) \times 10^{-11}$ cm^3 s^{-1}, and, assuming statistical breakdown of a long-lived complex, the rate constant for the formation of the $NO_2^{\ddagger}$ complex, $k_{1,cf}$ is $(7.4 \pm 1.0) \times 10^{-11}$ cm^3 s^{-1}. The slower O_2 exchange was measured three different ways, yielding three rate constants whose average is $k_{2,x} = (2.9 \pm 0.5) \times 10^{-12}$ cm^3 s^{-1}. The results are compared with earlier isotope exchange experiments and discussed in the context of measured and calculated high pressure recombination and vibrational relaxation rate constants.

I. INTRODUCTION

Radical–radical or radical–molecule reactions often proceed via strongly bound, but unstabilized, intermediates[1,2] that may (i) redissociate to reactants; (ii) dissociate exothermically to other products; or (iii) be collisionally stabilized to form a stable adduct. Understanding processes (i) and (ii) requires a knowledge not only of the energetics and quantum states of the adduct but also of the transition states between the adduct and reactants as well as products. Isotope exchange reactions are well suited to probe the rate of formation of the unstabilized intermediate, particularly if the isotope effect is small, i.e., if the isotopic label has a negligible effect on the elementary reaction rate constants. Except for a statistical factor that accounts for the ratio of total to observable exchanges, the isotope exchange rate constant is equal to the high-pressure limit, k^{∞}, of the second-order rate constant for the formation of the adduct.

If and when it is possible to reach k^{∞} experimentally by raising the pressure of inert gas, or when it is possible to use other labels for reactants such as vibrational excitation—assuming this has little effect on k^{∞}—one may have three independent measurements of k^{∞}. These may also be compared with semiempirical calculations of statistical theories or with trajectory calculations.

In the case of O + NO recombination, all four approaches had been taken, but earlier isotope exchange experiments[3] gave results about an order of magnitude lower than those of high pressure recombination experiments,[4] vibrational relaxation of NO($v = 1$) by O[5] and calculations using the adiabatic channel method.[6] The present reinvestigation of the rate of ^{18}O + NO isotope exchange removes this discrepancy.

For the $O + O_2$ recombination, fewer data are available. There is no major discrepancy between isotope exchange experiments in a flow reactor,[3] steady-state photolysis,[7] and high pressure recombination[8] experiments. Calculations using a simplified form of the adiabatic channel method have yielded larger rate constants for high pressure recombination[6] and vibrational relaxation[9] and suggest that the $^{18}O + O_2$ isotope exchange rate be remeasured. Furthermore, trajectory calculations[10,11] have raised the question whether the simple statistical factor of 2 is applicable in this case.

We report the results of such experiments carried out in a discharge-flow apparatus using a modulated molecular beam mass spectrometer for detection of labeled (^{18}O) and unlabeled species.

II. EXPERIMENTAL

A. Flow apparatus

The flow apparatus used here has been described before,[12,13] and the relevant portions are shown in Fig. 1(a). To permit study of the exchange reactions at short times, the 25 mm i.d. Pyrex flow tube was lengthened to extend the reaction zone to within 2 cm of the mass spectrometer sampling orifice, and the inner walls were coated with halocarbon wax (Halocarbon Products #15-00) to inhibit losses of O atoms. The injector was periodically lubricated with halocarbon oil (Halocarbon Products #56) to ease movement and inhibit wall losses on its outer surface. Helium flows were controlled with Nupro S-series valves and measured with calibrated Tylan mass flowmeters (Tylan FM360) and capillary pressure-drop manometers. Reagent flows were determined by rate of pressure rise in calibrated volumes, and all pressures were measured with calibrated pressure transducers (Validyne DP-7).

Nitric oxide (Matheson) was purified by slow passage through two traps [#1 molecular sieve at 203 K (dry ice/isopropanol), #2 ascarite at 113 K (liquid nitrogen/isopentane)], collected at room temperature to 1 atm pressure in a Pyrex bulb, frozen out at 77 K (liquid nitrogen) and degassed. $^{18}O_2$ was made by electrolysis of $H_2{}^{18}O$ (97% atom purity, YEDA Research and Development Company, Ltd., Weizmann Institute of Science) and stored in a Pyrex bulb with an appendage which was immersed in liquid nitrogen before and during use to trap water vapor. Helium (Matheson, 99.995%), was passed through a copper wool oven at 1173 K, followed by a molecular sieve trap in liquid nitrogen to remove hydrocarbons and H_2O. Oxygen-16 (Matheson

[a] Visiting professor, permanent address: Isotope Department, the Weizmann Institute of Science, Rehovoth, Israel.

 0021-9606/85/161648-09$02.10

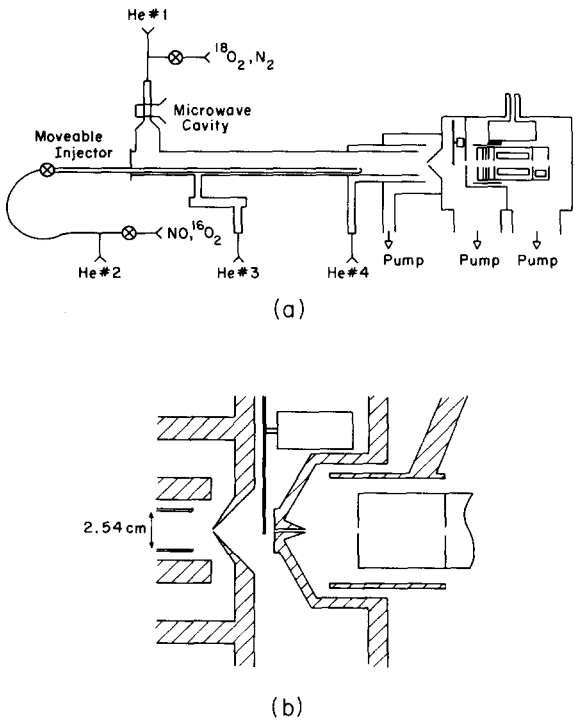

FIG. 1. (a) Diagram of apparatus. (b) Scale drawing of interface between the flow reactor and the mass spectrometer. Sampling orifice sealing device not shown.

Extra Dry 99.6%) and nitrogen (Matheson UHP 99.999%) were used without further purification. Typical gas flow rates provided average flow velocities v of 2100 cm/s at a total pressure of 0.9 Torr. Reactant concentrations were $[NO] = (0.5 \text{ to } 8)\times 10^{12}$; $[^{16}O_2] = (0.5 \text{ to } 11)\times 10^{13}$; $[^{18}O_2] = (0.5 \text{ to } 1.5)\times 10^{13}$; $[^{18}O] = (0.8 \text{ to } 2.0)\times 10^{12}$ cm^{-3}.

B. Modulated molecular beam mass spectrometer (MMBMS)

The geometry of the molecular beam forming elements is shown in Fig. 1(b). The sampling orifice (1.0 mm diam $\times$0.2 mm long) was made of 304 stainless steel and had a frontal half-angle of 55 ° permitting an open 45 ° cone behind the orifice. A retractable orifice sealing device [not shown in Fig. 1(b)] allowed work on the flow apparatus without disturbing the vacuum system. A second orifice (0.9 mm diam $\times$0.2 mm) collimated the beam such that it traversed the coaxially mounted ion source (Extranuclear Laboratories, #041-1 with #020-0 controller) and mass spectrometer rod assembly (Extranuclear Laboratories, #7-162-8 with ELFS plate) without surface collisions. The tube attached to this orifice (2.0 mm diam $\times$20 mm long) reduced effusion between the two pumping chambers by a factor of 5 without hindering passage of the beam, and a third orifice on the ionizer (3.1 mm diam) further decreased the flux of nonbeam particles into the mass spectrometer.

Each chamber was pumped by a 6 in. oil diffusion pump (Edwards Diffstak #160M, 800 ℓ/s with Santovac 5) backed by a 15 CFM rotary pump (Welch Duo-seal #1397). Air bleeds in the backing lines reduced backstreaming from the mechanical pumps. Rapid pumping of condensable gases was provided by a copper tube surrounding the ionizer which was conductively coupled to a liquid nitrogen trap. Two infrared lamps (GE#QH500T3) mounted internally provided bakeout capability. Although the total base pressure was limited to $(1\text{–}3)\times 10^{-6}$ Torr due to an intermittent leak in the trap, the system was otherwise reasonably clean, and detection limits were acceptable as discussed below.

The beam chopper consisted of a dc motor,[14] a speed controller,[15] and an aluminum chopping wheel (10 teeth, 26.4 cm diam, 1/32 in. thick). Chopper status was sensed by an IR LED/phototransistor pair (GE#H13A1-102) mounted in the vacuum system. All leads to the sensor and motor were individually shielded, and the motor was surrounded by a robust aluminum mount to eliminate brush contact noise. Chopper speed stability was checked with a Tektronics 2465 oscilloscope and found to be better than $\pm$ 0.2% for a period of a few minutes; about 0.5% over a day's run.

C. Mass spectrometer/data acquisition system

The electron impact ion source was operated with low emission (2 mA) to reduce background signals due to heating of the source, and low electron energy (20 eV nominal) to minimize fragmentation. No detectable contributions at 16 amu from $N^{16}O$, nor at the 18 amu from $^{18}O_2$ were observed at the concentrations used here. A small amount of fragmentation of $^{16}O_2$ was observed at larger concentrations and taken into account in the data analysis for these experiments. The resolution settings were a compromise between peak shapes and separation, and the resulting performance is indicated by the vacuum system residual scan shown in Fig. 3(a), taken when the aforementioned leak was relatively small. The sensitivities obtained for NO, O_2, and O were 6, 3, and 1.5 (counts/s)/(10^9 cm^{-3}) in the flow tube, respectively. Detection limits for $N^{16}O$, $^{16}O^{18}O$, ^{16}O, and ^{18}O were 2×10^9, 5×10^9, 2×10^{10}, and 6×10^{10} cm^{-3}.

The data acquisition system shown schematically in Fig. 2 permits phase-sensitive measurements of mass spectrometer signals[16] using ion counting detection to obtain maximum signal-to-noise ratios.[17] This has been done before[18] using a multichannel analyzer with up-down counting capability. Here, we present a simpler system using a lock-in amplifier and two gated scalers. Ions were detected with an electron multiplier (Johnston MM-1) whose output could be routed either to an electrometer (Extranuclear Laboratories #031-2, preamp #032-5), or to a pulse preamp/discriminator (EG&G#1182) for ion counting. The pulse stream from the discriminator was connected to two channels of a multiscaler (Tennelec 535P). The chopper status signal was sent to the reference channel of a lock-in amplifier (Keithley Autoloc 840), whose monitor output was used to generate two complementary time-delayed gating signals for the multiscaler, one of which was also fed to the external clock input. Pulses were counted in both channels for a preset number of chopper cycles and read out by the buffer/interface module (Tennelec #588) into the computer (Hewlett Packard 9816) for accumulation, processing, and display. The computer also controlled the quadrupole power supply (Extranuclear Laboratories #011-1) via a 12 bit D/A converter (Hewlett Packard 6140B with #69321B).

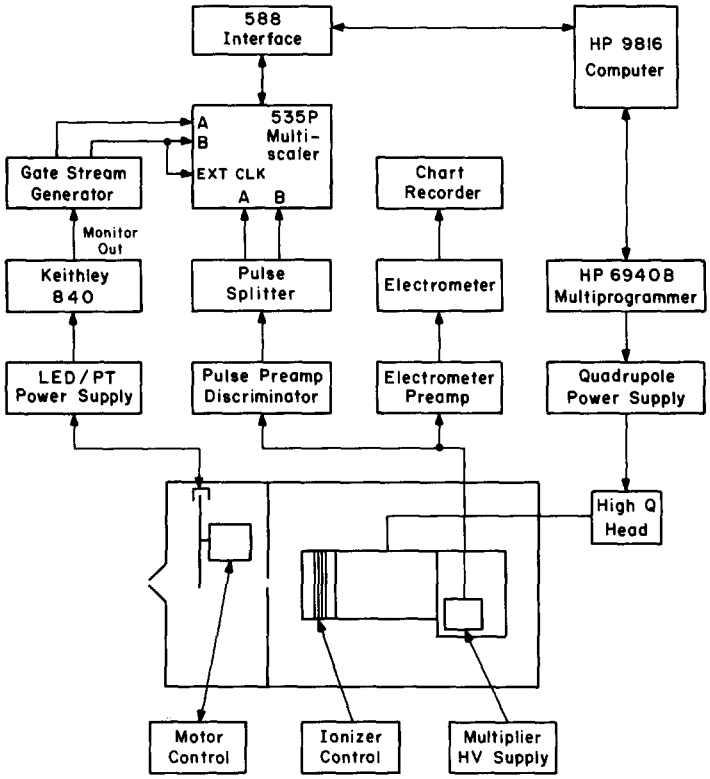

FIG. 2. Diagram of data acquisition/mass spectrometer control electronics.

Vacuum system background gases produce ion signals which are constant in time as long as the extraction characteristics of the ion source are not affected by the ionization of the modulated beam. The low electron energies used here preclude ionization of the primary beam gas (helium), and low emission currents further reduce space charge effects.[19,20] The background rejection capability of this system is demonstrated in Fig. 3(b). For this scan, the sampling orifice was opened to the flow tube which contained 0.9 Torr of flowing helium. The signals plotted are differences between the two counter channels, one of which may be interpreted as beam + background, the other as background only. Comparison with Fig. 3(a) shows that background signals are nulled to within the statistics. Small net signals are present at 18 and 36 amu due to residual water and HCl in the flow tube. The latter were due to unrelated experiments using HCl, conducted just prior to these scans. Several attempts were made to reduce the water signal by baking the molecular sieve traps and the flow tube, but all were unsuccessful. This background level was monitored carefully during all phases of the experiments to be described and found to be independent of whether the microwave discharge was on or off. In kinetic experiments, data were collected by sequencing the spectrometer through a table of predetermined peak centers. Integration times were increased to 7 s per peak compared to the ~0.25 s intervals used for the scans shown in Figs. 3 and 5.

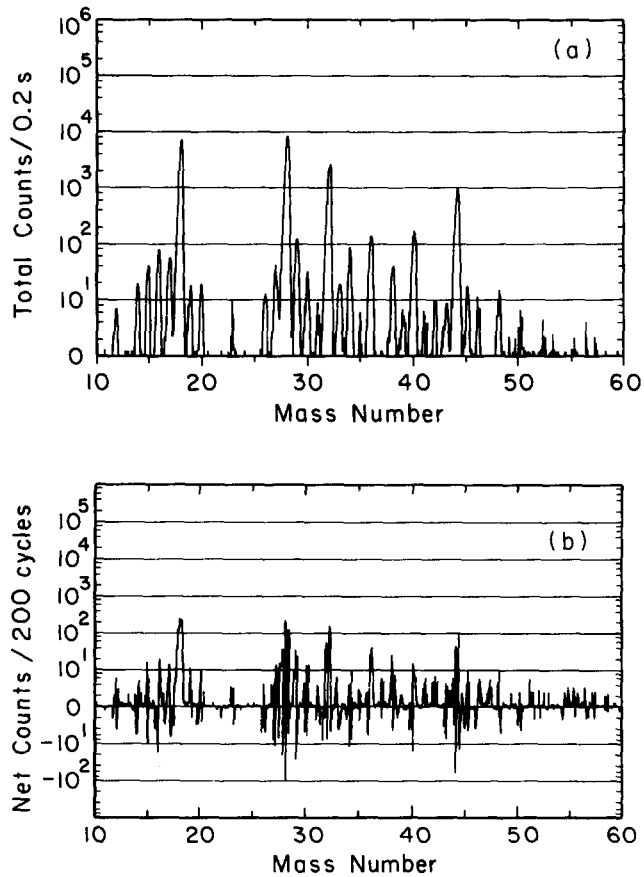

FIG. 3. Sample mass spectra. (a) Vacuum system residual, sampling orifice closed, $P \sim 3 \times 10^{-8}$ Torr, chopper not running. (b) Flow reactor residual with 0.9 Torr of flowing helium, sampling orifice open, chopper running at 400 Hz, difference signals plotted.

III. DATA ANALYSIS AND PROCEDURE

A. O + NO

In the absence of interfering secondary processes, the kinetics of the reaction

$$^{18}O + N^{16}O \rightleftarrows {}^{16}O + N^{18}O, \quad k_{1f} = k_{1r} = k_{1,x} \qquad (1)$$

are governed by the rate equation

$$d[N^{16}O]/dt = -k_{1,x}[N^{16}O][^{18}O] + k_{1,x}[N^{18}O][^{16}O],$$

where small primary isotope effects have been ignored. Similar rate expressions hold for $N^{18}O$, ^{18}O, and ^{16}O. All four equations are easily solved if one observes that O atoms and NO are separately conserved and that $\Delta[N^{16}O] = \Delta[^{18}O]$. The exact solution for $[N^{16}O]$ is found to be

$$[N^{16}O]_t = [N^{16}O]_e + ([N^{16}O]_0 - [N^{16}O]_e) \times \exp\{-k_{1,x}([NO]_T + [O]_T)t\},$$

where $[N^{16}O]_0$ and $[N^{16}O]_e$ are the initial and equilibrium concentrations of $N^{16}O$, respectively, and $[NO]_T$ and $[O]_T$ are the total, conserved NO and O concentrations. $[N^{16}O]_e$ is determined by $[N^{16}O]_0$, $[^{18}O]_0$, $[^{16}O]_0$, and is given by[30]

$$[N^{16}O]_e = [N^{16}O]_0 \times \{1 - [^{18}O]_0/([NO]_T + [O]_T)\}.$$

The expressions for the other species are similar. Note that the behavior is exponential even for comparable reactant concentrations and that to extract $k_{1,x}$ from first-order rate measurements one should plot k^I against $[NO]_T + [O]_T$.

In practice, however, the exchange with molecular oxygen

$$^{16}O + {}^{18}O_2 \rightleftarrows {}^{18}O + {}^{16}O{}^{18}O, \quad k_{2f} = 2k_{2r} = k_{2,x} \qquad (2)$$

interferes with this simple interpretation. The effect on the concentrations of $N^{16}O$ and ^{18}O is illustrated by the computer simulation presented in Fig. 4. ^{16}O atoms produced in the primary $^{18}O + N^{16}O$ process are converted back to ^{18}O by reaction with undissociated $^{18}O_2$ and react again with $N^{16}O$. As a result, both the $N^{16}O$ and ^{18}O atom profiles depart from "O_2 free" chemistry; $[^{18}O]$ falls short of equilibrium and begins to turn back, while $[N^{16}O]$ decreases monotonically beyond its equilibrium value. At short times, however, these effects are relatively small. In this work, we have restricted the range of reaction times appropriately for each $[NO]_T + [O]_T$ and analyzed the data for the O + NO reaction using O_2 free chemistry.

The MMBMS was calibrated for $N^{16}O$, ^{16}O, and ^{18}O atoms for each day's run. Small measured flows of NO were quantitatively converted to ^{16}O atoms by reaction with excess N, produced by substituting N_2 for $^{18}O_2$ in the microwave discharge. $[N_2]$ was usually 5×10^{14} cm^{-3}, which produced $[N] = (5\text{–}10)\times10^{12}$ cm^{-3} for 20–30 W forward discharge power, and [N] was monitored at 14 amu to ensure that $[N] \gg [NO]$. Signals at 14, 16, and 30 amu were measured under three conditions: discharge off with NO (a), discharge on with NO (b), and without NO (c). Mass scans of the flow tube contents in each case are shown in Fig. 5. $N^{16}O$ and ^{16}O sensitivities were obtained from condition (a) and the (b) − (c) difference, respectively, for several [NO] to expose any nonlinearities; none were found. ^{18}O sensitivity was obtained by discharging $^{18}O_2$ and comparing the changes in the 18 and 16 amu signals upon addition of NO. These changes generally agreed to better than 5%.

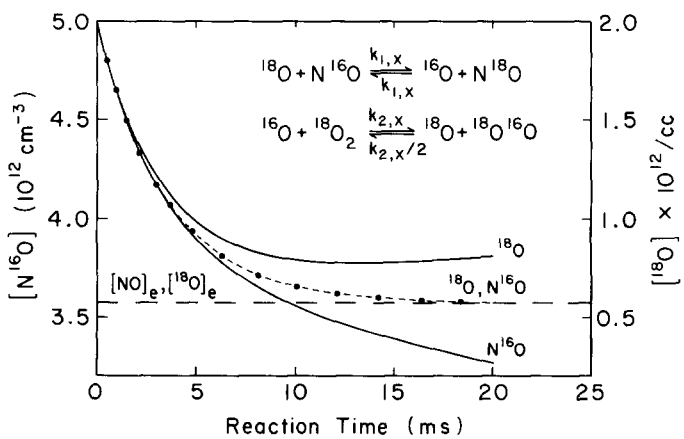

FIG. 4. Computer simulation of $^{18}O + N^{16}O \rightleftarrows {}^{16}O + N^{18}O$ exchange with (—) and without (- · -) the effects of the $^{16}O + {}^{18}O_2 \rightleftarrows {}^{18}O + {}^{16}O_2$ reaction. (- -) calculated equilibrium values of $[N^{16}O]$ and $[^{18}O]$. Rate constants used: $k_{1,x} = 4\times10^{-11}$, $k_{2,x} = 3\times10^{-12}$ cm^3 s^{-1}, $[^{18}O_2]_0 = (9 \text{ or } 0)\times10^{12}$ cm^{-3}.

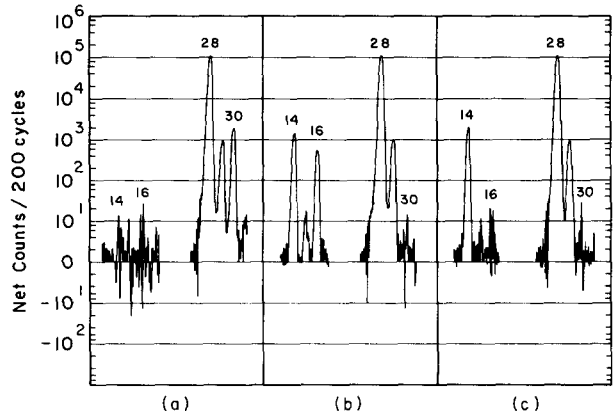

FIG. 5. Mass spectrum segments recorded during O atom calibration, $[NO] \simeq 2\times10^{12}$ cm^{-3}. (a) N_2, NO on, discharge off. (b) N_2, NO on, discharge on. (c) N_2 on, NO off, discharge on.

The N + NO reaction was also used as a movable source to measure O atom wall losses; $k_w(O)$ was found to be less than 1 s^{-1}. The injector effect was measured by monitoring ^{18}O at several injector positions without adding NO and was found to be negligibly small as well.

Each first-order rate measurement required the initial values for $[N^{16}O]$, $[^{16}O]$, and $[^{18}O]$ as well as their variations over a suitable range of reaction times. After establishing an $^{18}O_2$ flow, a measured amount of NO was added through the injector, and background for ^{16}O and ^{18}O as well as initial $^{18}O_2$ and $N^{16}O$ signals were recorded. The NO flow was diverted and remeasured while the microwave discharge was turned on and allowed to stabilize, permitting mass spectrometer measurements of $[O^{16}]_0$ and $[^{18}O]_0$. NO was then reintroduced and $[N^{16}O]$, $[^{16}O]$, and $[^{18}O]$ were monitored at about ten points over a predetermined range of injector positions. Finally, $[^{16}O]_0$ and $[^{18}O]_0$ were rechecked by temporarily diverting the NO, and the discharge was turned off, allowing final mass spectrometer measurements of $[N^{16}O]_0$. Pre- and post-exchange measurements generally agreed to within a few percent. A sample of raw $^{18}O + N^{16}O$ exchange data and the asymptotic signal values calculated from initial concentrations is presented in Fig. 6(a). $N^{18}O$ signals were not used in these experiments due to interference from $^{16}O_2$.

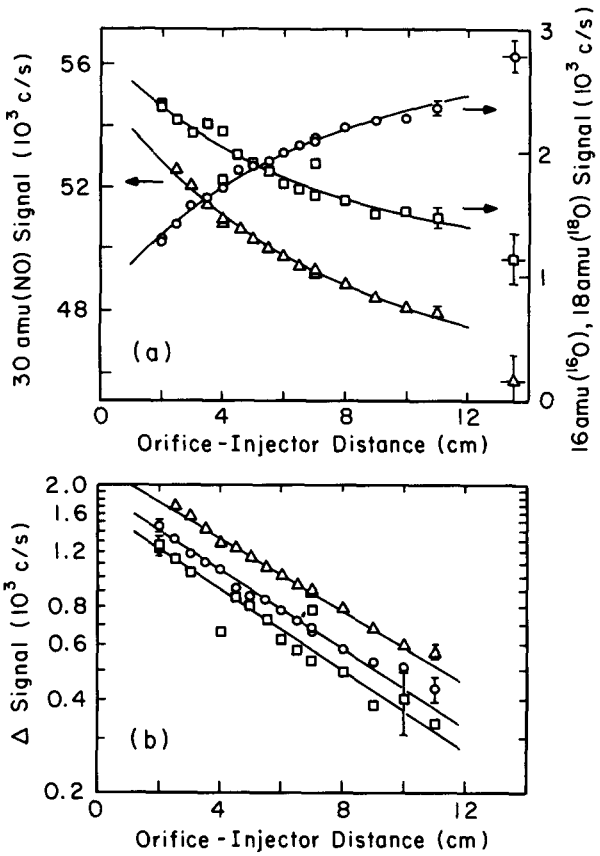

FIG. 6. Sample $^{18}O + N^{16}O \leftrightarrows {}^{16}O$ exchange data, $[NO]_T + [O]_T = 9.6\times10^{12}$ cm^{-3}. ($\triangle$) = $N^{16}O$, (O) = ^{16}O, ($\square$) = ^{18}O. Error bars indicate 1 σ statistical uncertainty. (a) Raw signals of $N^{16}O$, ^{16}O, ^{18}O vs injector distance. Note different scales for $N^{16}O$ and O atoms. Lines are fits from (b), calculated equilibrium values, $[X]_e$, indicated on right. (b) $\ln([X] - [X]_e)$ vs injector distance, presented as pseudo-first-order decays. $N^{16}O$ signals $\times 1/4$. Lines are precision weighted fits.

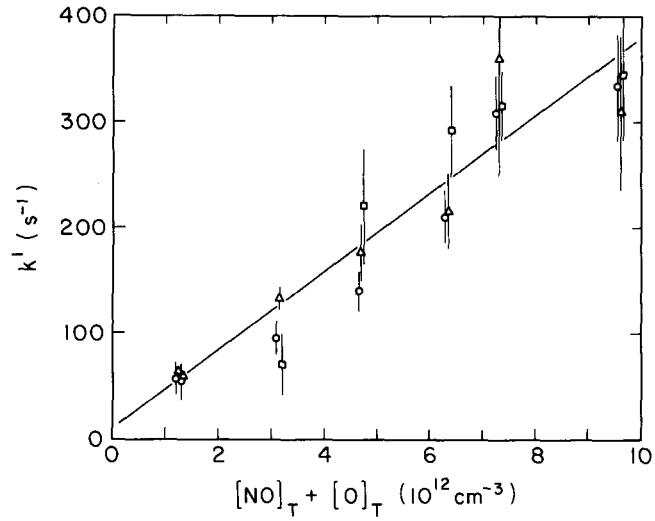

FIG. 7. Bimolecular plot of k^I vs $[NO]_T + [O]_T$ for $^{18}O + N^{16}O \leftrightarrows {}^{16}O + N^{18}O$ exchanges. ($\triangle$) = $N^{16}O$, (O) = ^{16}O, displaced left, ($\square$) = ^{18}O displaced right. Error bars show total 1 σ uncertainty for each k^I. Line is precision-weighted fit, yields $k_{1,x} = (3.7 \pm 0.3)\times10^{-11}$ cm^3 s^{-1}.

First-order rate constants were obtained from precision-weighted, semilog least-squares fits[21] of $[X] - [X]_e$ vs orifice-injector distance for $X = N^{16}O$, ^{16}O, and ^{18}O in seven, seven, and five experiments, respectively. This weighting procedure discriminated further against longer reaction times. The signal differences associated with the exchange shown in Fig. 6(a) and their semilog fits are shown in Fig. 6(b). The 19 k^I's thus obtained were corrected for axial and radial diffusion[22] (the largest adjustment was $+7\%$) and plotted against $[NO]_T + [O]_T$ (Fig. 7) to obtain the bimolecular rate constant and its statistical uncertainty using a precision-weighted, least-squares fit, $k_{1,x} = (3.7 \pm 0.3)\times10^{-11}$ cm^3 s^{-1}. The error bars include the effect of uncertainties in $[X]_e$ on k^I as well as the precision of the individual k^I fits at the 1σ level.

B. $O + O_2$

Three different methods were employed to determine the rate constant for O atom exchange with O_2. The first, which we call the NO-tracer method, provides some insight into the probable flaw in the earlier work.[3] The two other techniques were based on direct observations of ^{18}O atoms exchanging with O_2 and consequent production of $^{16}O^{18}O$.

1. NO as tracer

As discussed above, the $^{18}O + N^{16}O$ exchange process is perturbed at longer reaction times by recycling of ^{16}O to ^{18}O by undissociated $^{18}O_2$. In fact, the faster $O + NO$ process can be considered to be nearly in equilibrium, with $[^{16}O]$ and $[^{18}O]$ determined by reaction with $^{18}O_2$. Thus, $[N^{16}O]$ can serve as a probe for monitoring the progress of the $^{16}O + {}^{18}O_2$ reaction. Modification of the simple kinetic scheme presented above to include reaction (2) is straightforward:

$$\begin{aligned} d[^{16}O]/dt &= (-d[^{18}O]/dt) \\ &= k_{1,x}\{[^{18}O][N^{16}O] - [^{16}O][N^{18}O]\} \\ &\quad - k_{2,x}\{[^{16}O][^{18}O_2] - [^{18}O][^{16}O^{18}O]/2\}, \end{aligned}$$

where reactions involving $^{16}O_2$ have been neglected due to its small concentration in these experiments. We note (see Fig. 4) that $[^{18}O]$ (and $[^{16}O]$) are roughly constant for a time after $[N^{16}O]$ passes its equilibrium value. Exploiting this and realizing that under these conditions $[^{16}O][^{18}O_2] \sim 50 \times [^{18}O][^{16}O^{18}O]$ we obtain

$$d[N^{16}O]/dt \simeq -k_{2,x}[^{16}O][^{18}O_2]$$

so that $k_{2,x}$ may be extracted from plots of $\Delta[N^{16}O]$ against Δt, as long as $[^{16}O]$ is roughly constant over the interval Δt. One such plot is shown in Fig. 8. Five determinations of $k_{2,x}$ were made, all with roughly the same values of $[^{16}O]$ and $[^{18}O_2]$. Our result for $k_{2,x} = (3.0 \pm 0.3)\times10^{-12}$cm^3 s^{-1} from this method is the simple average of the five values.

2. Direct O-atom exchange

The $^{18}O + {}^{16}O_2$ exchange was studied directly in separate experiments substituting $^{16}O_2$ for NO. The kinetics must now include the reaction

$$^{18}O + {}^{16}O_2 \rightleftarrows {}^{16}O + {}^{16}O^{18} \qquad (3)$$

as well as reaction (2), giving the following set of rate equa-

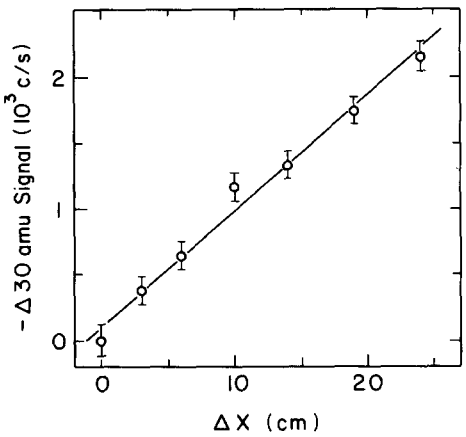

FIG. 8. Sample $^{16}O + {}^{18}O_2 \leftrightarrows {}^{18}O + {}^{16}O^{18}O$ exchange data from NO-tracer method. $\Delta x = 0$ corresponds to orifice-injector distance of 18 cm, $-\Delta 30 = 0$ corresponds to a 30 amu signal of $\sim 35\,000$ counts/s. Line is unit-weighted fit, yields $k_{2,x} = 2.8 \times 10^{-12}$ cm^3 s^{-1}.

tions:

$$d[^{16}O_2]/dt = -k_{2,x}[^{18}O][^{16}O_2] + (k_{2,x}/2)[^{16}O][^{16}O^{18}O] \quad (4)$$

$$d[^{18}O_2]/dt = -k_{2,x}[^{16}O][^{18}O_2] + (k_{2,x}/2)[^{18}O][^{16}O^{18}O] \quad (5)$$

$$d[^{16}O^{18}O]/dt = \{d[^{16}O_2]/dt + d[^{18}O_2]/dt\} \quad (6)$$

$$d[^{16}O]/dt = -d[^{18}O]/dt = d([^{18}O_2] - [^{16}O_2])/dt.$$

Conservation conditions ($[^{16}O_2] + [^{16}O^{18}O] + [^{18}O_2] = [O_2]_T$, and $[^{16}O] + [^{18}O] = [O]_T$) again reduce the number of independent variables, and the exact solution for $[^{16}O]$ is

$$[^{16}O]_t = [^{16}O]_e + ([^{16}O]_0 - [^{16}O]_e) \times \exp\{-k_{2,x}([O_2]_T + [O]_T/2)t\},$$

where $[^{16}O]_e$ is given by

$$[^{16}O]_e - [^{16}O]_0 = \{1 + ([^{16}O_2]_0 - [^{18}O_2]_0)/[O_2]_T - 2[^{16}O]_0/[O]_T\} \times \{([O]_T/2)/(1 + [O]_t/2[O_2]_T)\}$$

which are similar to the solutions obtained earlier. The behavior of the homonuclear molecular oxygen components is more complicated and not needed here; that of $[^{16}O^{18}O]$ will be derived below. Experiments similar to those already described for the O + NO exchange were carried out except that no restriction to short reaction times was required. Similar data analysis techniques were applied after correcting ^{16}O data for $^{16}O_2$ fragmentation; the largest such correction represented about 5% of the equilibrium ^{16}O signal. Typical raw and reduced exchange data and the corresponding bimolecular plot are shown in Figs. 9(a), 9(b), and 10. The rate constant obtained from this method was $k_{2,x} = (2.6 \pm 0.3) \times 10^{-12}$ cm^3 s^{-1}.

3. $^{16}O\,^{18}O$ product appearance

The two reactions (2) and (3) comprise an interesting dynamic system in which ^{16}O and ^{18}O are continuously interchanged, producing $^{16}O^{18}O$ at the expense of $^{16}O_2$ and $^{18}O_2$. The time scales for the ($^{18}O \rightarrow {}^{16}O$) and ($^{16}O_2 \rightarrow {}^{16}O^{18}O \leftarrow {}^{18}O_2$) conversion processes are very different under our typical experimental conditions where $[O]_T \ll [O_2]_T$. The molecular conversion is barely underway by

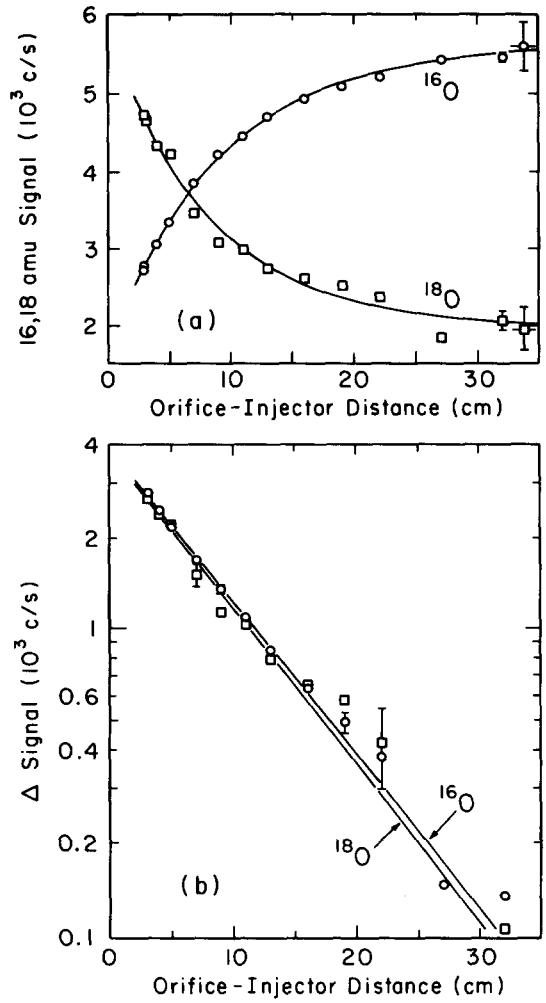

FIG. 9. Sample $^{18}O + {}^{16}O_2 \leftrightarrows {}^{16}O + {}^{16}O^{18}O$ exchange data from observations of O atoms, $[O_2]_T + [O]_T/2 = 8.6 \times 10^{13}$ cm^{-3}. (O) = ^{16}O, (□) = ^{18}O cm^{-3}. Error bars indicate 1 σ statistical uncertainty. (a) Raw signals vs injector distance. Lines are fits from (b), calculated equilibrium values, $[X]_e$, indicated on right. (b) $\ln([X] - [X]_e)$ vs injector distance, presented as pseudo-first-order decays. Lines are precision-weighted fits.

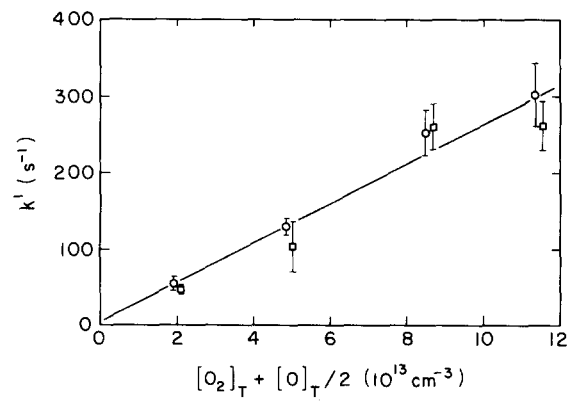

FIG. 10. Bimolecular plot of k' vs $[O_2]_T + [O]_T/2$ for O atom measurements of $^{18}O + {}^{16}O_2 \leftrightarrows {}^{16}O + {}^{16}O^{18}O$ exchanges. (O) = ^{16}O displaced left, (□) = ^{18}O displaced right. Error bars show total 1 σ uncertainty for each k'. Line is precision-weighted fit, yields $k_{2,x} = (2.6 \pm 0.3) \times 10^{-12}$ cm^3 s^{-1}.

the time equilibrium between the atomic species is reached, and the reaction continues producing $^{16}O^{18}O$ long afterwards. The time behavior of $[^{16}O^{18}O]$ can therefore be used to measure $k_{2,x}$.

From Eqs. (4), (5), and (6) above, one obtains

$$d[^{16}O^{18}O]/dt = k_{2,x}\{[^{18}O][^{16}O_2] + [^{16}O][^{18}O_2] - [^{16}O^{18}O][O]_T/2\}.$$

Since $[^{16}O_2]$ and $[^{18}O_2]$ are nearly constant, we assume $[^{16}O_2] = [^{16}O_2]_0$ and $[^{18}O_2] = [^{18}O_2]_0$, and writing $\beta = [^{18}O_2]_0/[^{16}O_2]_0$, we find that

$$\begin{aligned} v \cdot d[^{16}O^{18}O]/dx &= k_{2,x}\{[^{16}O_2]_0([^{18}O] + \beta[^{16}O]) \\ &\quad - [^{16}O^{18}O][O]_T/2\} \\ &= k_{2,x}\{U\}, \end{aligned} \tag{7}$$

where we have used $dt = dx/v$, v being the average flow velocity.

Time profiles of 34 amu signals, (34), obtained during O atom exchange experiments were plotted and fitted piecewise as indicated in Fig. 11(a) yielding two or three values of $d(34)/dx$ per exchange. These were converted to $d[^{16}O^{18}O]/dx$ using mass spectrometer sensitivities for $^{18}O_2$ at 36 amu. Means for $[^{16}O^{18}O]$, $[^{18}O]$, and $[^{16}O]$ over these intervals were obtained in similar fashion from averages of (34), (18), and (16), respectively. Values of $v \cdot d[^{16}O^{18}O]/dx$ were plotted against the concentration product $\{U\}$ on the right side of Eq. (7) in the spirit of a bimolecular plot [Fig. 11(b)], the slope of which gave $k_{2,x} = (3.0 \pm 0.3) \times 10^{-12} \times 10^{-12}$ cm^3 s^{-1}.

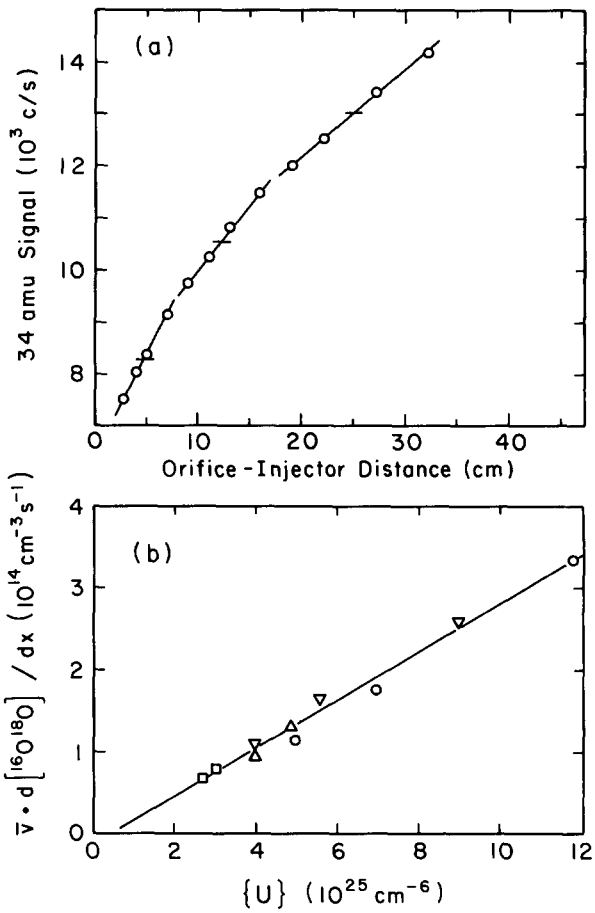

FIG. 11. (a) Sample $^{18}O + {}^{16}O_2 \leftrightarrows {}^{16}O + {}^{16}O^{18}O$ exchange data from $^{16}O^{18}O$ product appearance method, $[O_2]_T + [O]_T/2 = 8.6 \times 10^{13}$ cm^{-3}. Raw 34 amu signals vs injector distance, statistical uncertainty indicated by data point size. Lines are piecewise, unit-weighted fits, dashes show average values over each interval. (b) Pseudo-bimolecular plot for $^{16}O^{18}O$ product measurements of $^{18}O + {}^{16}O_2 \rightarrow {}^{16}O + {}^{16}O^{18}O$ exchange. $\{U\}$ is defined in Eq. (7). Uncertainty for each point is about 15% = 1σ. Different symbols indicate different experiments, (○) = data from (a). Line is unit-weighted fit, yields $k_{2,x} = (3.0 \pm 0.3) \times 10^{-12}$ cm^3 s^{-1}.

IV. RESULTS AND DISCUSSION

Table I lists all related experimental and calculated rate constants for the O + NO and O + O_2 reactions. Except for the trajectory studies for O + O_2,[10,11] the theoretical entries are based on two semiempirical techniques due to Quack and Troe.[6] The full adiabatic channel model (ACM) is generally considered capable of predicting rate constants to within a factor of 2. A single parameter, α, related to the rate of change of energy eigenvalues along the reaction path is available for fitting to experimental data. Values of α near 1 Å^{-1} are considered physically reasonable. Departures from $\alpha \sim 1$ Å^{-1} indicate more complicated behavior. The simpler maximum free energy/variable transition state theory (MFE) is an approximation to ACM and is considerably easier to use. MFE generally produces rate constants that are upper limits to ACM results (see recombination data) although there are exceptions [see $O_2(v)$ relaxation data]. MFE theory also has one parameter, γ, which plays a role similar though not identical to that of α in ACM. Two values of γ, 0.75α and 0.75 Å^{-1}, are usually used. The first provides the closest match between ACM and MFE results; the second is based on the value $\alpha = 1$ Å^{-1} recommended for *a priori* application of ACM.

A. O + NO

Our result for the $^{18}O + N^{16}O$ isotope exchange reaction, $k_{1,x} = (3.7 \pm 0.5) \times 10^{-11}$ cm^3 s^{-1}, is considerably larger than the 1.8×10^{-12} first reported by Herron and Klein,[3] who also used a fast flow reactor/mass spectrometer system, but whose anomalously low value is explained by interference from the $^{16}O + {}^{18}O_2$ reaction. We estimate that the $[^{18}O]$ in their studies was probably about 10^{15} cm^{-3}, easily driving the $^{18}O + N^{16}O$ exchange to "equilibrium" within 1–2 ms. The ^{16}O atoms produced then exchanged with undissociated $^{18}O_2$ causing additional consumption of $N^{16}O$ as we have observed in our experiments. This continuing change in $N^{16}O$ or $N^{18}O$ would have been attributed to the $^{18}O + N^{16}O$ exchange.

To compare our result with other measurements, we convert the exchange rate constant to that for complex formation, which should be the rate constant for recombination at high pressure. Conversion of $k_{1,x}$ to $k_{1,cf}$, however, requires some knowledge of the exchange mechanism. If the $NO_2^\dagger$ intermediate is long-lived and ejects ^{16}O or ^{18}O statistically when it decomposes, $k_{1,x}$ should be one half of $k_{1,cf}$. If the exchange occurs by direct atom transfer, $k_{1,cf}$ will be equal to $k_{1,x}$. Intermediate behavior will give $k_{1,cf}$ between these extremes.

TABLE I. Summary of relevant experimental and calculated rate constants for O + NO and O + O_2 near 300 K.

Process	k (10^{-11} cm^3 s^{-1})	Method	Ref.
		O + NO	
Isotope exchange (expt)	0.18	discharge-flow/MS	3
Isotope exchange (expt)	3.7 ± 0.5	discharge-flow/MS	This work
Recombination (expt)	3.0	high pressure, up to 200 atm	4
Recombination (calc)	(1.8,2.8,2.1)[a]	ACM ($\alpha = 1.3$ Å^{-1}), MFE ($\gamma = 0.75\alpha$), MFE($\gamma = 0.75$ Å^{-1})	6
Recombination (calc)	5.8[b]	MFE($\gamma = 0.75$ Å^{-1})	5
NO vib. relaxn. (expt)	6.5	laser-induced IR fluorescence	5
NO vib. relaxn. (calc)	(1.7,1.8)[a]	ACM ($\alpha = 1.3$ Å^{-1}), MFE ($\gamma = 0.75$ Å^{-1})	29,9
NO vib. relaxn. (calc)	5.0[b]	MFE ($\gamma = 0.75$ Å^{-1})	5
		O + O_2	
Isotope exchange (expt)	$0.10, 0.17^{+0.10}_{-0.06}$	discharge-flow/MS	3,26
Isotope exchange (expt)	0.17[c]	photolysis, ratio to k_3	7
Isotope exchange (expt)	0.29 ± 0.05	discharge-flow/MS	This work
Isotope exchange (calc)	0.27,0.12	quasiclassical trajectory studies	10,11
Recombination (expt)	0.28	high pressure, up to 200 atm	8,28
Recombination (calc)	(0.25,0.32,0.63)	ACM ($\alpha = 0.35$ Å^{-1}), MFE($\gamma = 0.75\alpha$), MFE ($\gamma = 0.75$ Å^{-1})	6
O_2 vib. relaxn. (calc)	(0.70,0.54)	ACM ($\alpha = 0.35$ Å^{-1}), MFE ($\gamma = 0.75$ Å^{-1})	9

[a] NO_2 ground state only.
[b] Includes bound electronically excited states.
[c] Adjusted for $k_3 = 9.3 \times 10^{-12}$ cm^3 s^{-1}; see the text, Sec. IV B.

A simple density of states calculation[23] suggests that $NO_2^\dagger$ near its dissociation energy has a lifetime of about 200 periods of its lowest frequency vibration if only the ground electronic state is formed. Inclusion of bound electronic states increases this estimate by about a factor of 2. This should be long enough to ensure the statistical ejection of O atoms, and we conclude that $k_{1,cf} = 2k_{1,x} = (7.4 \pm 1.0) \times 10^{-11}$ cm^3 s^{-1}.

The measurements of the O + NO recombination at pressures up to 200 atm by Hippler *et al.*[4] suggest $k^{\infty}_{1,\mathrm{rec}} = 3.0 \times 10^{-11}$, more than a factor of 2 below our $k_{1,cf}$. There is, however, some doubt concerning how closely the high pressure limit can be approached experimentally due to diffusion and cage effects.[24] The vibrational relaxation experiments of Fernando and Smith,[5] $k_{1,\mathrm{rlx}} = (6.5 \pm 0.4) \times 10^{-11}$ cm^3 s^{-1} suggest a higher value for $k^{\infty}_{1,\mathrm{rec}} = (7.5 \pm 0.5) \times 10^{-11}$ in excellent agreement with our $k_{1,cf}$. The rlx→rec conversion is based on the ratio of calculated rate constants for high pressure NO + O recombination (5.8×10^{-11}) and vibrational relaxation of NO($v = 1$) by O(5.0×10^{-11}) presented in Ref. 5, which include contributions from bound electronically excited states of $NO_2^\dagger$. This ratio is likely to be more reliable than its component parts, which are only accurate to within a factor of 2. We conclude, therefore, that the agreement among recent studies of the O + NO system is quite good.

B. O + O_2

We have obtained three separate estimates for $k_{2,x}$ in this work: (3.0 ± 0.3), (2.6 ± 0.3), and $(3.0 \pm 0.3) \times 10^{-12}$ cm^3 s^{-1} from the NO tracer, direct O atom observations and $^{16}O^{18}O$ product measurement methods, respectively. It has been estimated that microwave discharges of O_2 produce comparable quantities of O atoms and metastable $O_2(^1\Delta)$,[5] which is notoriously resistant to quenching by either wall or intermolecular collisions. Reactions involving $O_2(^1\Delta)$ would differ from ground state reactions not only in energy but in the states of the $O_3^\dagger$ intermediate which may be accessible, e.g., only triplet states of O_3 are formed directly from $O(^3P) + O_2(^1\Delta g)$, whereas singlet and triplet states are accessible from $O(^3P) + O_2(X\,^3\Sigma_g^-)$. As a result, the rate constants for O atom exchange may be different. In our oxygen-only experiments, there is much more O_2 present in the form of $^{16}O_2$ reactant added through the movable injector. The effect of $O_2(^1\Delta)$ on the observed reaction rate would then be diluted due to nearly resonant electronic energy transfer between $^{18}O_2$ and $^{16}O_2$,[25] reducing the fraction of total O_2 in the singlet state. Although no such dilution occurs for the NO tracer experiments, the rate constants obtained for the three methods were indistinguishable within experimental uncertainties, indicating that any perturbation due to $O_2(^1\Delta)$ is probably small. We report $k_{2,x} = (2.9 \pm 0.5) \times 10^{-12}$ cm^3 s^{-1} as a precision-weighted average of the rate constants obtained from these three methods, and quoted 1σ uncertainty includes statistical uncertainties plus 10% estimated total undetected errors.

This value is nearly three times larger than that obtained by Herron and Klein[3] and the most recent quasiclassical trajectory calculations of Varandas and Murrell.[11] The earlier trajectory studies of Stace and Murrell[10] used a simpler potential surface, but are in better agreement with our measurement. Brennen and Niki[26] have also studied the $^{16}O + {}^{18}O_2$ exchange in a flow tube/mass spectrometer system. By selecting comparable $[^{16}O]_0$ and $[^{18}O_2]_0$, they extracted $k_{2,x'} = (1.7^{+1.0}_{-0.6}) \times 10^{-12}$ cm^3 s^{-1} from the behavior of $[^{18}O_2]$ second-order plots at short times. Jaffe and Klein[7]

used a photolysis technique to measure the exchange rate relative to the rate of the reaction

$$O + NO_2 \rightarrow O_2 + NO, \quad k_3. \tag{8}$$

They obtained $k_{2,x} = 1.0\times10^{-12}$ using $k_3 = 5.4\times10^{-12}$. Employing the current value[27] for k_3 (9.3×10^{-12}) increases their $k_{2,x}$ to 1.7×10^{-12}, still somewhat below our result. The remaining discrepancy may be due to missing chemistry in the model used to extract the rate constant from the photolysis data. We point out that the temperature variation of $k_{2,x}$ observed by Jaffe and Klein over small temperature range (298–402 K), was attributed entirely to that assumed for the reference rate constant, k_3, i.e., the ratio $k_{2,x}/k_3$ did not vary with temperature. Since the currently accepted value for k_3 is temperature independent, their observations indicate that $k_{2,x}$ is also.

The relationship between the exchange and complex formation rate constants for the $O + O_2$ system is not as straightforward as for $O + NO$. The estimated lifetime of O_3 is shorter than $NO_2^\dagger$ by about a factor of 4, only about 40 vibrational periods, indicating that some mixture of complex formation and direct exchange mechanisms may be involved. The first trajectory studies of Stace and Murrell[10] suggested that direct collisions dominate, but later calculations by Varandas and Murrell[11] implied that long-lived (2.5 ps) complexes play a more important role in the exchange process. In view of this uncertainty, it seems prudent to conclude that $k_{2,x} \leqslant k_{2,cf} \leqslant 2k_{2,x}$ or $(2.9 \leqslant k_{2,cf} \leqslant 5.8)\times10^{-12}$ $cm^3\ s^{-1}$, although it is probably closer to the upper than to the lower limit.

This range of values lies somewhat above both the experimental high pressure recombination rate measurements of Hippler and Troe[8] and of Croce De Cobos and Troe,[28] both of whom found $k^{\infty}_{2,rec} = (2.8 \pm 1.0)\times10^{-12}$, and Quack and Troe's[6] theoretical value of $k^{\infty}_{2,rec} \sim 2.5\times10^{-12}$. The value of $\alpha = 0.35$ required to fit the ACM calculations to their experimental result is considered anomalously low, so that the choice $\gamma = 0.75$ A^{-1} for the MFE predictions is questionable. If, however, $k^{\infty}_{2,rec}$ is really closer to our upper limit for $k_{2,cf} = 5.8\times10^{-12}$ $cm^3\ s^{-1}$, then α would be 0.5–0.6. The MFE ($\gamma = 0.75$ $Å^{-1}$) result appears more reasonable and approaches the value predicted for the $O_2(v = 1) + O$ vibrational relaxation rate constant, which has not been measured at 300 K. Nevertheless, it does not seem likely that the present differences between the various experimental and calculated rate constants can be resolved by refinement of the theory of recombination. Further work is needed on the relationship of $k_{2,x}$ to $k^{\infty}_{2,rec}$ using trajectory calculations on realistic potential energy surfaces accounting for the outcomes of all encounters as a function of the lifetimes of the collision complexes. This should also be done for $k_{1,x}$ and $k^{\infty}_{1,rec}$ to provide a base line for the comparison. For k_1, the well-known excited states ($^2B_2$, $^2B_1$, $^2A_2$, and perhaps $^4A_2$ and $^4B_2$) should also be included to confirm the results of MFE theory.[5]

ACKNOWLEDGMENTS

We would like to thank Dr. J. L. Durant, Mr. J. A. McCaulley, and Mr. J. M. Thomas of our group and Dr. J. T. Herron of NBS for useful discussions. This work was supported by AFOSR Grant 80 0207 and ARO Grant DAAG2981K0050.

[1] M. J. Howard and I. W. M. Smith, Prog. React. Kinet. **12**, 55 (1983).
[2] F. Kaufman, J. Phys. Chem. **88**, 4909 (1984).
[3] J. T. Herron and F. S. Klein, J. Chem. Phys. **40**, 2731 (1964).
[4] H. Hippler, C. Schippert, and J. Troe, Int. J. Chem. Kinet. Suppl. **1**, 27 (1975).
[5] R. P. Fernando and I. W. M. Smith, Chem. Phys. Lett. **66**, 218 (1979).
[6] M. Quack and J. Troe, Ber. Bunsenges. Phys. Chem. **81**, 329 (1971).
[7] S. Jaffe and F. S. Klein, Trans. Faraday Soc. **62**, 3135 (1966).
[8] H. Hippler and J. Troe, Ber. Bunsenges. Phys. Chem. **75**, 27 (1971).
[9] M. Quack and J. Troe, Ber. Bunsenges. Phys. Chem. **81**, 160 (1977).
[10] A. J. Stace and J. N. Murrell, J. Chem. Soc. Faraday Trans. 2 **74**, 2182 (1978).
[11] A. J. C. Varandas and J. N. Murrell, Chem. Phys. Lett. **88**, 1 (1982).
[12] J. B. Jeffries, J. A. McCaulley, and F. Kaufman, Chem. Phys. Lett. **106**, 111 (1984).
[13] J. A. McCaulley, S. M. Anderson, J. B. Jeffries, and F. Kaufman, Chem. Phys. Lett. **115**, 180 (1985).
[14] TRW/Globe type CLL #313A102-25 75 V dc motor with high temperature armature, vacuum bearings and high altitude brushes.
[15] Dart model #251-05E, modified to allow grounding of one motor lead, output inductively filtered.
[16] W. L. Fite, Int. J. Mass Spectrom. Ion Phys. **16**, 109 (1975).
[17] F. M. Harris, G. W. Trott, T. G. Morgan, A. G. Brenton, E. E. Kingston, and J. H. Beynon, *Mass Spectrometry Reviews 1984* (Wiley, New York, 1984), Vol. 3, p. 209.
[18] J. M. Calo and A. D. Bailey, Rev. Sci. Instrum. **45**, 1325 (1974).
[19] G. O. Brink, Rev. Sci. Instrum. **37**, 857 (1966).
[20] Extranuclear Laboratories instruction manual for 041-1 ionizer.
[21] R. J. Cvetanovic, D. L. Singleton, and G. Paraskevopoulos, J. Phys. Chem. **83**, 50 (1979).
[22] F. Kaufman, Prog. React. Kinet. **1**, 1 (1961); R. L. Brown, J. Res. Natl. Bur. Stand. **83**, 1 (1978); L. F. Keyser, J. Phys. Chem. **88**, 4750 (1984).
[23] W. Forst, *Theory of Unimolecular Reactions* (Academic, New York, 1973), pp. 61, 105.
[24] H. Hippler, V. Schubert, and J. Troe, J. Chem. Phys. **81**, 3931 (1984).
[25] I. T. N. Jones and K. D. Bayes, J. Chem. Phys. **57**, 1003 (1972).
[26] W. Brennen and H. Niki, J. Chem. Phys. **42**, 3725 (1965).
[27] D. L. Baulch, R. A. Cox, P. J. Crutzen, R. F. Hampson, Jr., J. A. Kerr, J. Troe, and R. T. Watson, J. Phys. Chem. Ref. Data **11**, 330 (1982).
[28] A. E. Croce De Cobos and J. Troe, Int. J. Chem. Kinet. **16**, 1519 (1984).
[29] M. Quack and J. Troe, Ber. Bunsenges. Phys. Chem. **79**, 170 (1975).
[30] This expression is correct for $[N^9O]_0 = 0$. The general result is

$$[N^{16}O]_e = [N^{16}O]_T \times \left\{1 - \frac{[^{18}O_0] + [N^{18}O\rangle]_0}{[0]_T + [NO]_T}\right\}.$$